Characterization of granular Phase Change Materials for thermal energy storage applications in fluidized beds

M.A. Izquierdo-Barrientos[a], C. Sobrino[a], J.A. Almendros-Ibáñez[b,c,*], C. Barreneche[d], N. Ellis[e], L.F. Cabeza[d]

[a] *Universidad Carlos III de Madrid, ISE Research Group, Thermal and Fluid Engineering Department, Avda. de la Universidad 30, 28911 Leganés, Madrid, Spain*
[b] *Escuela de Ingenieros Industriales, Dpto. de Mecánica Aplicada e Ingeniería de Proyectos, Castilla-La Mancha University, Campus universitario s/n, 02071, Albacete, Spain*
[c] *Renewable Energy Research Institute, Section of Solar and Energy Efficiency, C/ de la Investigación s/n, 02071, Albacete, Spain*
[d] *GREA Innovació Concurrent, Universitat de Lleida Edifici CREA, Pere de Cabrera s/n, 25001 Lleida, Spain*
[e] *Department of Chemical and Biological Engineering, University of British Columbia, Vancouver V6T 1Z3, Canada*

Abstract

This work investigates commercially available granular phase change materials (PCMs) with different transition temperatures for the use of thermal-energy storage systems in fluidized beds. The hydrodynamic characteristics of granular PCMs were tested in cylindrical-3D and planar-2D fluidized beds. The density, particle size distribution and angle of repose were measured for various PCM materials. Further attrition studies were conducted with changes in particle surface from abrasion, which were characterized using a Scanning Electron Microscope (SEM). The results indicate that some materials with smaller particle size and thinner supporting structure can lose the

*Corresponding author. Tel.:+34 967599200-ext:8204
Email address: jose.almendros@uclm.es (J.A. Almendros-Ibáñez)

paraffin during the fluidization process, when paraffin is in a liquid state. As a consequence, the particles agglomerate, and the bed defluidizes. For all of the tested materials, only GR50 (with a transition temperature of 50°C) properly fluidizes when the paraffin is in the liquid state and has shown to endure $>$ 75 hours of continuous operation and 15 melting-solidification cycles in a fluidized bed. Additional differential scanning calorimetry (DSC) measurements of the cycled particles did not show a decrease in energy storage capacity of the granular PCM, which corroborates that there is no loss of material after $>$ 75 hours of fluidization.
Keywords: PCM, Thermal energy storage, Fluidized beds, Angle of repose, DSC

1. Introduction

To satisfy the global energy demand, thermal energy storage (TES) is a promising technique to complement the variability in renewable energy supplies and increase the market demand (IEA, 2012). In this context, phase change materials (PCM), which use latent heat storage, are an attractive alternative to sensible heat materials in either shell-and-tube storage systems (Yang et al., 2016) or dual-media (solid particles-fluid) energy storage tanks because they provide high storage density (Xu et al., 2015). In this case, the PCM is encased in capsules of different geometries and sizes. The advantage of the encapsulation is its applicability for both liquid and air as heat transfer fluids because they are easily handled and maintain their macroscopic solid state during the solid-liquid transition. Encapsulated PCMs in small particles (micro-encapsulation) have high heat transfer area between the particles

and the heat transfer fluid.

In the literature, there are studies of packed beds of macro-encapsulated spheres of PCM with diameters of a few centimeters and water as the heat transfer fluid (Xia et al., 2010; Oró et al., 2013). In addition to these bound PCMs, granular phase-changing composites with small particle diameters (1-3 mm) have been tested in latent heat thermal-storage packed beds (Rady, 2009a; Izquierdo-Barrientos et al., 2013) using air as the heat transfer fluid and in combination with a compressed-air energy storage system (Peng et al., 2015). Pitié et al. (2013) also studied the potential use of granular PCMs in a high-temperature (500-750 °C) circulating fluidized bed. They concluded that the PCM would help to reduce the temperature in the tubes and circulation rate of the particles, although granular materials for such high temperatures remain to be developed and manufactured.

Previously, we have published different works on granular phase change materials for low-temperature storage applications in bubbling fluidized beds (Izquierdo-Barrientos et al., 2013, 2015a,b, 2016), as an alternative to the traditional packed beds. The authors have observed that a fluidized bed of granular PCM has higher charging efficiencies during the charging process than a fluidized bed of sand or a packed bed of the identical granular material. The heat transfer coefficient between the particles and a heated surface, which is immersed in the bed, is also notably augmented in a fluidized bed with granular PCM because of the latent heat of the particles, when the bed works at approximately the transition temperature of the PCM. In all previous works, the authors used the same commercial product available from Rubitherm: "*GR bound PCM*", which consists of an inorganic matrix in

which the PCM is adsorbed and rigidly bounded irrespective of whether the PCM is solid or liquid form. Different paraffins can be used as PCM in the granular material, depending on the transition temperature desired. In our case, we used the material GR50 with a transition temperature of approximately 50 °C. This material was properly fluidized at temperatures below and above this transition temperature and did not present agglomeration problems. Although it suffered some attrition after 75 hours of continuous operation with 15 charging-discharging cycles, no evidence of loss of PCM was observed.

In the present work, we tested the same commercial product, "*GR bound PCM*" from Rubitherm, but commercialized with different phase change temperatures: GR42 and GR80, with transition temperatures of approximately 42 °C and 80 °C, respectively. The first experimental observations showed that GR42 and GR80 did not properly fluidized at temperatures above the transition temperature: the particles agglomerated, and the bed was defluidized.

To understand the agglomeration behavior of various granular phase-changing composites, where two of three materials have agglomeration problems when they are heated in a fluidized bed, the hydrodynamic characteristics of the materials in fluidized beds are studied in this paper. The angle-of-repose measurements, attrition testing and SEM observations are used to understand the different behaviors of these materials. The DSC measurements are finally performed to check the differences in thermal behavior of the suitable material to fluidize after several heating cycles.

2. Materials

The commercial product employed in this work is "*GR bound PCM*", which is commercialized by Rubitherm (www.rubitherm.eu) and suitable for low-temperature energy storage applications (−10 °C to 90 °C). Three different materials with three different phase change temperatures were tested: GR42, GR50 and GR80. The number corresponds to their approximate phase change temperature T_{pcm}. Figure 1 shows a picture of different PCMs and a picture of the silica sand in the experiments of Izquierdo-Barrientos et al. (2013), which is a common sensible storage material and was used as a reference material. The external appearance of the granular PCMs is similar to any other granular material, regardless of whether the PCM is in the liquid or solid state. The granular PCM is composed of paraffin ($\sim$ 30 % wt.), which is the phase-changing component, and a natural porous material. The paraffin is different in each material to get the desired transition temperature. The inorganic component behaves similarly to a sponge, where the organic PCM is adsorbed during the manufacturing process. The PCM is rigidly bound to the inorganic matrix regardless of whether the PCM is in the solid or liquid state. The granular material has been developed to be easily handled. These granular PCMs are available in two sizes with particle diameters of 1-3 mm (coarser size) and 0.2-0.6 mm (finer size). These materials were used by different researchers for thermal-energy storage applications in fixed (Rady, 2009a; Izquierdo-Barrientos et al., 2013) and fluidized beds Izquierdo-Barrientos et al. (2013, 2015a).

[Figure 1 about here.]

2.1. Density, size distribution and minimum fluidization velocity

The two main properties of any granular material to be fluidized are their density and size, which can be categorized according to Geldart (1973) to predict the fluidization behavior of these materials.

The particle density of the granular PCMs has been determined using a helium pycnometer AccuPyc 1340 of micromeritics. This device uses the gas displacement method to measure the volume occupied by the sample, and the density is calculated as the ratio of the mass to its volume; the mass is invariably measured on a discrete device. Table 1 shows the density of different granular PCMs. There is no noticeable difference among the different granular PCMs. The density of the granular PCMs is notably lower than other typical materials in fluidized beds. Izquierdo-Barrientos et al. (2013, 2015a) experimentally and numerically compared the thermal behavior of two granular materials (finer GR50 and sand) in a fluidized-bed thermal-storage system. The density of the sand in these works was $\rho = 2632.3\,\mathrm{kg/m^3}$. Izquierdo-Barrientos et al. (2013) observed that the lower density of GR50 enabled higher efficiencies because of the lower necessary mass flow rate to fluidize the particles.

[Table 1 about here.]

Figures 2(a) and 2(b) show the cumulative particle size distribution, which was measured using the equipment Retsch AS-200-control with a sieve analysis for the finer and coarser granular PCMs, respectively. In these figures, the percentage in passing mass versus the sieve size is represented. Figure 2(a) shows that the finer GR50 has a larger percentage of larger particles

than the other two finer materials, whereas the coarser GR42 has a larger percentage of particles with a size under 1 mm (see Figure 2(b)). Table 2 indicates the mean particle size of each material, which was calculated with the particle size distribution, and its standard deviation. For comparison purposes, the mean particle size of the sand that Izquierdo-Barrientos et al. (2013) used in their experiments is also indicated. The larger mean particle size of the finer GR50, compared to GR42 and GR80, indicates a thicker boundary structure of this material in comparison with the other two.

[Figure 2 about here.]

[Table 2 about here.]

The minimum fluidization velocity U_{mf} of the three thinner materials was determined by measuring the pressure drop across the bed as a function of the superficial gas velocity. The minimum fluidization velocity is commonly defined as the intersection of the horizontal fluidized bed line and the sloping packed bed line (Sanchez-Delgado et al., 2011). Table 3 shows U_{mf} of the finer PCMs materials. U_{mf} of the coarser PCMs was not experimentally measured because they are higher than the maximum superficial gas velocity that our facility can supply. These velocities were estimated according to Wen and Yu (1966).

[Table 3 about here.]

Figure 3 shows the original Geldart diagram (Geldart, 1973) where different particle types are indicated. In this diagram, the finer granular PCMs in this work are indicated with solid points, which are clearly particles type

B. This type of particles fluidizes with a vigorous bubbling behavior and presents a good circulation and mixing of solids. The coarser granular PCMs are indicated with empty symbols. These particles belong to type D particles, which do not easily fluidize, and large amounts of gas are required. This type of particles can be used in spouted beds and/or fixed and moving beds, which is beyond the scope of this work. In this figure, the sand used by Izquierdo-Barrientos et al. (2013) is indicated with a star. Although this point is in group D particles, it is notably close to Geldart B. Izquierdo-Barrientos et al. (2013) experimentally observed a particle behavior similar to that of type B with a bubbling behavior.

Considering Figure 3, the finer granular PCMs appear appropriate to use in a bubbling fluidized bed and will be the selected material in the fluidization experiments in this paper. Although GR42 and GR80 have smaller particle size than GR50, they belong to group B particles and are far from the limit of group C particles (cohesive particles), where the interparticle forces are strong and hinder the fluidization process. Thus it is speculated that the interparticle forces are not the dominante force in causing the observed agglomeration in the finer materials GR42 and GR80. The required air flow rate to fluidize the coarser granular PCM would be too high, which discard their use in a bubbling fluidized bed. In the following section, we describe the behavior of the finer GR42 and GR80 in two experimental setups: cylindrical-3D and planar-2D fluidized beds. The 2D bed enables us to observe the interior of the bed.

[Figure 3 about here.]

3. Fluidization experiments

3.1. Experimental set-ups

The finer granular PCMs were fluidized in two experimental set-ups. First, the materials were tested in a cylindrical-3D fluidized bed (identical to that used by Izquierdo-Barrientos et al. (2013, 2015a)). Second, to visually corroborate the results in the 3D facility, a planar-2D fluidized bed was used, which enables a visual inspection of the fluidization process.

The cylindrical-3D fluidized bed is illustrated in Figure 4. The bed consisted of a cylindrical tube of ID 200 mm stainless steel with 2 mm thick walls. A fine mesh screen was mounted at the bottom of the distributor plate to prevent the solid particles from entering the plenum chamber. The air entered the plenum of the column and flowed into the bed through a distribution plate with a thickness of 1.5 mm, which contained 300 perforations with a diameter of 2 mm, which resulted in a 3% open area. The instrumentally monitored section of the test apparatus was 500 mm high and insulated with 20-mm-thick glass wool. Additionally, the column was insulated with a 10-mm-thick thermal insulator. The expanded freeboard had an internal diameter of 300 mm. The air flow was supplied by a blower with a variable mass flow rate and heated by electrical heaters, which were regulated by a PID controller before flowing into the column. Type K thermocouples were used to measure the temperature at specific locations in the test section and plenum chamber. At these locations, the pressure variations could be measured using pressure sensors with two different ranges: 100 mbar and 1 bar.

[Figure 4 about here.]

Figure 5 shows a scheme of the planar-2D fluidized bed, which is identical to that used by (Mahecha-Botero et al., 2011). The experimental apparatus is a two-dimensional fluidized column with inner dimensions of 310x16x510 mm, which was designed to operate at a maximum pressure of 2170 kPa. The fluidized bed was constructed of 43 mm thick steel plates. To view the fluidization phenomena, four tempered glass windows of 157-mm diameter and 25.4-mm thickness were used. The windows were placed in pairs on opposite faces of the column and maintained in place using silicon. Then, a gasket was placed outwards over the windows and steel plates to prevent the windows from sliding outwards. A metal mesh was used as the distributor, and additional mesh were used to prevent the backflow of particles, which would clog the bed fittings. The gas supply for the fluidized bed derived from the compressed air from the building air line and was preheated before entering the column by a heating tape. To control the inflow of gas into the fluidized bed, the flow rate was controlled by regulators and more precisely with needle valves.

[Figure 5 about here.]

3.2. Experimental results

Figure 6 shows the temperature profile obtained by Izquierdo-Barrientos et al. (2013) in the cylindrical-3D bed with finer GR50, which was fluidized at U/U_{mf} of 1.5, 2.0 and 2.5. The bed was filled with 5 kg of GR50, which resulted in a bed height at minimum fluidization conditions of approximately $H_{mf} \approx D = 20\,\text{cm}$. Four thermocouples measured the temperature at 2.5 cm, 7.5 cm, 12.5 cm and 17.5 cm above the distributor. Two additional

thermocouples measured the air temperature at the bed inlet, below the distributor, and at the exit. Three experiments were performed with three different flow rates: 375, 500 and 625 l/min, which corresponded with superficial gas velocities of 0.2, 0.27 and 0.33 m/s, respectively. Hence, according to the minimum fluidization velocity of the material GR50 (see Table 3), the experiments were performed at an excess gas velocity over minimum fluidization conditions of $U/U_{mf} = 1.5$, 2.0 and 2.5. In all cases, the air was heated to a temperature of 65°C, and the particles in the bed were heated for 2-3 hours. Then, the electrical resistance that heated the air was switched off, the air and particles were cooled, and the temperature was measured.

Three thermocouples at 7.5 cm, 12.5 cm and 17.5 cm above the distributor measured the identical temperature, which indicates the well-mixed state in the bubbling fluidized bed. Only the thermocouple near the distributor (2.5 cm above it) showed a higher temperature. This thermocouple could be affected by the air jets from the distributor and measured a temperature closer to the temperature of the inlet air (Rees et al., 2006).

[Figure 6 about here.]

Figure 7 shows the experimental results with the granular PCMs GR42 and GR80, which were tested under the identical experimental conditions of Izquierdo-Barrientos et al. (2013) with GR50, as shown in Figure 6. These materials have a smaller mean particle size than GR50 and consequently lower U_{mf}. Because the experiments with materials GR42 and GR80 were performed with constant superficial gas velocities of $U = 0.20$, 0.27 and 0.33 m/s, the excess velocities over minimum fluidization velocity with identical

gas flow rates are higher for the experiments with these materials. Contrary to the experimental results of the finer GR50 (Izquierdo-Barrientos et al., 2013), these materials did not properly fluidize when the temperature of the bed was higher than the transition temperature of each material (T_{pcm}). For example, in Figure 7(b) (GR80 with $\dot{V} = 375\,\mathrm{l/min}$), the bed behaved as a well-mixed tank up to nearly 80°C; however, beyond this temperature, the bed temperature progressively increased from the bottom to the top of the bed as in a plug-flow system. This behavior is typical of fixed beds and indicates that the bed was defluidized. This anomalous behavior appeared to be mitigated when the gas flow rate increased. For GR80 with a gas flow rate of $\dot{V} = 625\,\mathrm{l/min}$, which corresponds with an excess gas velocity of $U/U_{mf} = 4.4$, the bed was well mixed. Similar experimental results were obtained for GR42.

The differences in the hydrodynamic behavior of GR50, GR42 and GR80 are related with the different particle sizes and the characteristics of the natural porous material used as a matrix where the PCM material was bound. Because this supporting material might not be homogenous in composition, it could have different performances to avoid the leakage of the paraffin. In the case of GR42 and GR80, some paraffin leaked from the supportive structure; when paraffin melted during the charging process, it served as an adhesive, which made the granules stuck together and caused the bed to defluidize. Furthermore, when the bed was cooled below the phase change temperature, the paraffin solidified, and the fluidizing air broke the agglomerates and re-fluidized the bed. This re-fluidization only occurred for experiments where the air flow rate was sufficiently large to produce a vigorous bubbling of the

bed.

[Figure 7 about here.]

Additional experiments were performed in the planar-2D facility to observe the fluidization quality and bed behavior. Figure 8 shows three pictures where the bed interior is observed through one of the windows of the bed. Figure 8(a) shows the fluidization process of GR42 when the bed temperature was below the transition temperature of the material with a gas flow rate slightly higher than the minimum fluidization conditions. Small ascending bubbles were observed in the bed, which indicates that the bed was properly fluidized. In contrast, when the bed temperature was increased beyond T_{pcm}, the bubbles disappeared, and the particles appeared to become agglomerated, as observed in Figure 8(b). The increase in gas flow rate in an attempt to re-fluidize the bed was not successful in the 2D geometry. Instead, small channels were observed among the agglomerated particles (see Figure 8(c), which enabled the gas to by-pass the bed.

[Figure 8 about here.]

From the fluidization experiments, it is concluded that the materials GR42 and GR80 do not properly fluidize when the temperature of the bed is higher than their transition temperatures, i.e., 42°C and 80°C, respectively. When the granular PCM is above its transition temperature, the paraffin is in the liquid state and can leak out of the granule and act as a binder. Consequently, the particles tend to agglomerate, and the bed defluidizes.

4. Analysis of the granular PCMs

This section describes the results of additional experimental measurements to explain the observed differences in the fluidization process of the materials GR42 and GR80 when the temperature is above their transition temperature.

4.1. Angle of repose

The angle of repose is generally accepted as an indirect measurement of the characteristics of a bulk of particles to flow, i.e., its flowability (Geldart et al., 2006, 2009; Krantz et al., 2009). Geldart et al. (2009) shows that the inverse of the AOR is equivalent to the cohesion measured in a standard shear tester. Krantz et al. (2009) recommended dynamic testing (such as the AOR) to characterize particles to be used in applications where they are in motion (such as moving or fluidized beds), whereas static testing (such as shear cell methods) appears more appropriate to characterize powders to be used in packed beds. The angle of repose is commonly defined as the angle formed by a bulk of particles when they are poured through a funnel and forms a conical pile. The angle formed by the base of the cone and its generatrix is the angle of repose. Various authors (Antequera et al., 1994; Geldart et al., 2006) have proposed a limiting value of $AOR = 40°$. The bulk of particles above this value do not properly flow.

The angle of repose was measured for the three finer granular materials GR42, GR50 and GR80 in the identical device to that developed by Geldart et al. (2006). Figure 9 shows the angle of repose, which was obtained as the average value of seven runs, for the three materials at room tempera-

ture. Approximately 25 seconds were required to pour the entire sample. No noticeable differences appeared among the three materials. Because of the large error bars, it is not possible to delineate a clear trend with the angle of repose. Nevertheless, Chauvenet's criterion with a 90% confidence was applied to assess whether one piece of experimental data from the set of observations was likely spurious.

[Figure 9 about here.]

Figure 10 shows the variation of the angle of repose with temperature for the three materials to study a possible effect of the temperature on this parameter. No significant conclusions can be drawn because no remarkable changes appear in the AOR when the materials were heated beyond T_{pcm}. The angle of repose appeared unaffected by the temperature of the material. In all cases, except GR42 at a temperature above 60°C, the angle of repose was always under 40°, which is the limit proposed by Antequera et al. (1994) and Geldart et al. (2006) for a good flowability of the material.

[Figure 10 about here.]

During the angle-of-repose measurements, some problems were observed with the materials GR42 and GR80 at temperatures above their transition temperatures. When these materials were heated beyond T_{pcm}, their flowability decreased with signs of cohesiveness. In addition, the pouring time decreased to 12 seconds because the materials did not flow continuously but in clumps. For example, during the AOR measurement of GR80 at a temperature of 84°C, the particles flowed in blocks (Figure 11(a)), and some

electrostatic forces were observed in parts of the device (Figure 11(c)). Figures 11(b) and 11(d) show different problems of agglomerations and material blocks of GR42 at 62°C and 45°C, respectively. These problems, which affect the fluidization behavior of different materials, are not reflected in the AOR measurement.

[Figure 11 about here.]

4.2. Attrition tests

In fluidized beds, the vigorous bubbling in the bed can provoke the attrition of the particles. If the attrition is significant, the granular PCM particles can lose part of the paraffin inside the supporting structure of SiO_2. Two different attrition mechanisms are typically observed in fluidized beds: abrasion and fragmentation (Werther and Reppenhagen, 2013). In the fragmentation process, the particles are broken into smaller particles of similar sizes; in the abrasion process, fine particles are removed from the particle surface. Abrasion more frequently occurs in fluidized beds than fragmentation (Ray and Jiang, 1987; Pis et al., 1991).

In a previous study, Izquierdo-Barrientos et al. (2013) performed a cycling test to measure the particle size distribution of different samples of GR50, which were fluidized in the cylindrical 3D-facility as described in Section 3.1, during more than 75 hours of continuous fluidization and 15 heating-cooling cycles. The particle size distribution was measured after 3, 6, 9, 12 and 15 cycles. The particle size distribution slightly decreases with the number of cycles, although fragmentation was not observed.

To characterize the attrition resistance of granular PCMs and compare the behaviors of GR42 and GR80, which exhibited agglomeration problems, with

GR50, which was properly fluidized, attrition tests were performed. These tests also allowed to discard the fragmentation of particles during the fluidization process. The attrition testing apparatus follows the ASTM D5757-00 standard (ASTM D5757 - 00, 2006), which is a widely used standard procedure to characterize the attrition resistance of particles and powders (Wu et al., 2016; Zhao et al., 2000). It consists of four main stainless-steel components: the three-orifice (0.397 mm) distributor plate, attrition column (710 mm high, 35 mm), conically divergent/convergent freeboard settling chamber (630 mm high), and fine collector, which contains a ceramic filter (0.1 mm pore size). The unit was loaded with 50 g of the particulate sample and operated at 10 l/min of air at room temperature and room pressure for 5 hours.

The particle size distributions (PSDs) before and after the attrition tests for the three materials and their corresponding mean particle diameters with their standard deviations are shown in Figure 12. The distributions are Gaussian and have similar widths. Although the mean particle diameter is slightly higher for GR50, the shape of the distribution affects the defluidization of a fluidized bed more than the mean particle size (Lin et al., 2011). Figure 12 shows no particle fragmentation of the materials GR42 and GR80 (a bi-modal PSD should be obtained), so fragmentation is not the cause of the loss of paraffin and agglomeration of the bed when this type of granulates is fluidized.

[Figure 12 about here.]

The PSDs after the attrition tests indicate that the bed particles are only slightly smaller than the original ones. Considering Figure 12, it has been

proven that attrition increases the number of particles and decreases their size (the mean diameters decreased after the attrition tests). As a consequence, the PSDs are modified, being the degree of variation of the PSD after the attrition test notably similar for the three materials. Fine particles that are smaller than 50 μm were only detected for the finer GR80 with a fraction of 0.33% of the total mass, which is not significant. Nevertheless, due to the abrasion of materials, some leakages of the PCM might occur and affect the agglomeration of the material.

4.3. Scanning Electron Microscope (SEM) observations

One more test was performed to study the structure of the granular PCMs before and after fluidization. The microstructure of the three finer PCMs was examined using Scanning Electron Microscopy (SEM) on a Jeol 6490 LV electron microscope, which was equipped with an EDS detector (Oxford INCA Energy) and detectors for secondary and backscattered electrons. Figure 13 shows several SEM pictures for the materials GR42, GR50 and GR80 with a magnification of 2500 μm. The samples observed in the SEM were obtained before and after the fluidization experiments in the cylindrical 3D-bed in Figures 6 and 7.

The differences in contrast are related to the changes in conductivity of the material. No significant differences were detected between the initial and post-fluidization samples. Only the topography of the post-fluidization specimens, particularly GR42 and GR80, appeared softer than the initial ones, which may indicate that part of the paraffin leaked through the secondary structure. To corroborate that some paraffin was at the surface of the particles, an Energy Dispersive Spectroscopy (EDS) analysis was performed to

determine the C content at the surface. However, because of the interaction volume of the X-rays, C at the surface and C inside the particles were indistinguishable.

[Figure 13 about here.]

5. Differential Scanning Calorimetry (DSC) measurements

After the three finer granular PCMs were tested using two experimental facilities and different properties were measured, only the finer GR50 appeared appropriate for use in a fluidized bed for thermal-energy storage applications. The other two materials, GR42 and GR80, have agglomeration problems when the bed temperature is above their phase change temperature. These materials have smaller particle sizes than GR50. The external layer of porous material, which serves as a matrix to bind the PCM, may be thinner than the layer of GR50, and suffered from abrasion in the fluidization process, where some paraffin is lost and causes the particle agglomeration.

Izquierdo-Barrientos et al. (2013) analyzed and compared this material with sand in a fluidized bed for thermal-energy storage. GR50 was fluidized in fifteen charging-discharging cycles between ambient temperature and 65°C. The particles were fluidized in > 75 hours. After every three cycles, a sample of 250 g was extracted from the bed to measure the particle size distribution. They observed a slight decrease in mean particle size because of the abrasion.

To corroborate that the particles of GR50 in Izquierdo-Barrientos et al. (2013) did not lose the paraffin during the fluidization process, the extracted samples from the bed were analyzed in a Mettler Toledo DSC822e. A small mass of 20 mg of each sample of every three cycles was heated from 25°C

to 80°C at a rate of 0.5 K/min as recommended by various authors (Rady, 2009b; Giro-Paloma et al., 2015) in previous DSC studies, which measured the PCM, maintained them at this maximum temperature for ten minutes and subsequently cooled them to the initial temperature at the same rate. The process was repeated two times with a different small mass of 20 mg of each sample.

Table 4 summarizes the main results of the DSC analysis. The table shows the enthalpy changes and peak temperatures during the fusion (ΔH_{fus}) and solidification (ΔH_{sol}) processes. There is no decrease in enthalpy with the number of cycles. The differences between the initial and cycled samples (after 3, 6, 9, 12 and 15 cycles) are smaller than the DSC error and cannot be attributed to a loss of material.

Regarding the peak temperature, there are small differences between the initial and post-fluidized materials. For the unused material, the peak temperature during the fusion process is $T_{\text{peak}_{\text{fus}}} \approx 48$°C. After three cycles, this temperature decreased but remained approximately constant during all cycles with a value of $T_{\text{peak}_{\text{sol}}} \approx 45.4$°C. During the solidification process the peak temperature showed a similar behavior. A small hysteresis of 1°C was observed between the fusion and solidification processes. This value was maintained for all of the samples.

[Table 4 about here.]

6. Conclusions

The three finer granular PCMs in this work (GR42, 50 and 80) have optimal particle size and density to use in a bubbling fluidized bed. Never-

theless, the materials GR42 and GR80 have agglomeration problems during the fluidization process when the bed temperature is above their transition temperatures. As a consequence, the bed is de-fluidized, and the system behaves similarly to a plug flow system instead of a well-mixed tank. The agglomeration problems have been corroborated by visual inspection in a 2D fluidized bed. After measuring the angle of repose, performing an attrition test and observing the surface of the granular materials with a Scanning Electron Microscope, we conclude that there is no fragmentation of the granular PCMs during the fluidization process, and the cause of the agglomeration problems in GR42 and GR80 is some loss of paraffin because of the particle abrasion during the fluidization process. The paraffin leaks out, stays on the particle surface and acts as a binder. The finer GR50 does not exhibit this problem because it has a thicker boundary structure of SiO_2, which results in a higher mean particle size. The DSC measurements corroborate that the finer GR50 remains stable during 15 cycles of fusion-solidification in a bubbling fluidized bed.

Acknowledgments

Thanks to J. Canales-Vázquez from the Renewable Energy Research Institute of Albacete (Castilla-La Mancha University) for selflessly perform the SEM measurements.

The work is partially funded by the Spanish government (ENE2010-15403, ENE2011-22722 and ENE2015-64117-C5-1). The authors would like to thank the Catalan Government for the quality accreditation to their research groups GREA (2014 SGR 123). The study that led to these results has

received funding from the European Union's Seventh Framework Programme (FP7/2007-2013) under grant agreement n° PIRSES-GA-2013-610692 (INNOSTORAGE) and from the European Union's Horizon 2020 research and innovation programme under grant agreement No 657466 (INPATH-TES).

7. Notation

AOR	Angle of repose [deg]
d_p	Mean particle size [mm]
DSC	Differential Scanning Calorimetry
EDS	Energy Dispersive Spectroscopy
PCM	Phase Change Material
PSD	Particle Size Distribution
SEM	Scanning Electron Microscope
T	Temperature [°C]
T_{pcm}	Transition temperature of the granular PCM [°C]
T_{peak}	Peak temperature [°C]
U	Superficial gas velocity [m/s]
$\dot{V}$	Volumetric flow rate [l/min]

z Axial coordinate in the bed [cm]

7.1. Greek symbols

ΔH Enthalpy change [J/kg]

ρ Density [kg/m^3]

σ Standard deviation

7.2. Subscripts

fus Fusion

in Inlet conditions

mf At minimum fluidization conditions

sol Solidification

References

Antequera M.V.V., Ruiz A.M., Perales M.C.M., Muñoz N.M., Ballesteros M.R.J.C., 1994. Evaluation of an adequate method of estimating flowability according to powder characteristics. International Journal of Pharmaceutics, vol. 103, pp. 155-161.

ASTM 2006 Standard test method for determination of attrition and abrasion of powdered catalysts by air jets. Tech. Rep. D5757-00.

Brown R.C., Rasberry J.D., Overmann S.P., 1998. Microencapsulated phase-change materials as heat transfer media in gas-fluidized beds. Powder Technology, vol. 98, pp. 217-222.

Elsayed M.M., Megahed I.E., Wel-refaee M.M., 1988. Experimental testing of fluidized thermal storage bed, Solar & Wind Technology, vol. 5, pp. 15-25.

Geldart D., 1973. Types of gas fluidization. Powder Technology, vol. 7, pp. 285-292.

Geldart D., Abdullah E.C., Hassanpour A., Nwoke L.C., Wouters I., 2006. Characterization of powder flowability using measurement of angle of repose. China Particuology, vol. 4, pp. 104-107.

Geldart D., Abdullah E.C., Verlinden A., 2009. Characterisation of dry powders. Powder Technology, vol. 190, pp. 70-74.

Giro-Paloma J., Barreneche C., Martínez M., Sumiga B., Cabeza L.F., Fernández A.I., 2015. Comparison of phase change slurries: Physicochemical and thermal properties. Energy, vol. 87, pp. 223-227.

Izquierdo-Barrientos M.A., Sobrino C., Almendros-Ibáñez J.A., 2013. Thermal energy storage in a fluidized bed of PCM. Chemical Engineering Journal, vol. 230, pp. 573-583.

Izquierdo-Barrientos M.A., Sobrino C., Almendros-Ibáñez J.A., 2015. Energy storage with PCM in fluidized beds: Modeling and experiments. Chemical Engineering Journal, vol. 264, pp. 497-505.

Izquierdo-Barrientos M.A., Sobrino C., Almendros-Ibáñez J.A., 2015. Experimental heat transfer coefficients between a surface and fixed and fluidized beds with PCM. Applied Thermal Engineering, vol. 78, pp. 373-379.

Izquierdo-Barrientos M.A., Sobrino C., Almendros-Ibáñez J.A., 2016. Modeling the heat transfer coefficient between a surface and fixed and fluidized beds with phase change material. Journal of Heat Transfer: Transactions of the ASME, vol. 138, paper 072001.

Krantz K., Zhang H., Zhu J., 2009. Characterization of powder flow: Static and dynamics testing. Powder Technology, vol. 194, pp. 239-245.

Lin C.L., Peng T.H., Wang W.J., 2011. Effect of particle size distribution on agglomeration/defluidization during fluidized bed combustion. Powder Technology, vol. 207, pp. 290-295.

Mahecha-Botero A., Heseidi F., Nguyen A., Li T. and Grace J.R., 2010. Investigation of phase change volumetric flow in fluidized-bed reactors, in S.D. Kim, Y. Kang, J.K. Lee, Y.C. Seo (Eds.), Fluidization XIII: New Paradigm in Fluidization Engineering, Engineering Conference International, Article 73.

Oró E., Chiu J., Martin V., Cabeza L.F., 2013. Comparative study of different numerical models of packed bed thermal energy storage systems. Applied Thermal Engineering, vol. 50, pp. 384-392.

Peng H., Li R., Ling X., Dong H., 2015. Modeling on heat storage performance of compressed air in a packed bed system, Applied Energy, vol. 160, pp. 1-9.

Pis J.J., Fuertes A.B., Artos A., Suárez A., Rubiera F., 1991. Attrition of coal ash particles in a fluidized bed, Powder Technology, vol. 66, pp. 41-46.

Pitié F., Zhao C.Y., Baeyens J., Degrève J., Zhang H.L., 2013. Circulating fluidized bed heat recovery/storage and its potential to use coated phase-change-material (PCM) particles, Applied Energy, vol. 109, pp. 505-513.

Rady M., 2009a. Granular phase change materials for thermal energy storage: experiments and numerical simulations. Applied Thermal Engineering, vol. 29, pp. 3149-3159.

Rady M., 2009b. Study of phase changing characteristics of granular composites using differential scanning calorimetry. Energy Conversion and Management, vol. 50, pp. 1210-1217.

Ray Y.C., Jiang T.S., 1987. Particle attrition phenomena in a fluidized bed, Powder Technology, vol. 49, pp. 193-206.

Rees A.C., Davidson J.F., Dennis J.S., Fennell P.S., Gladden L.F.,Hayhurst A.N., Mantle M.D., Müller C.R., Sederman A.J., 2006. The nature of the flow just above the perforated plate distributor of a gas-fluidised bed, as imaged using magnetic resonance. Chemical Engineering Science, vol. 61, pp. 6002-6015.

Sánchez-Delgado S., Almendros-Ibáñez J.A., García-Hernando N., Santana D., 2011. On the minimum fluidization velocity in 2D fluidized beds. Powder Technology, vol. 207, pp. 145-153.

www.rubitherm.eu. Last accesed January, 2016.

Technology Roadmap. Solar Heating and Cooling. International Energy Agency (IEA), 2012. Available from www.iea.org (last accesed December 2015).

Wen C.Y., Yu Y.H., 1966. A generalized method for predicting the minimum fluidization velocity. AIChE Journal, vol. 12, pp. 610-612.

Werther J., Reppenhagen J., Attrition, in: W.C. Yang (Ed.), Handbook of Fluidization and Fluid-Particle Systems, Marcel Dekker Inc., New York (Chapter 8), 2013.

Wu D., Wu F., Gu Z., 2016. Catalyst attrition in an ASTM fluidized bed. Catalysis Today, vol. 264, pp. 70-74.

Xia L., Zhang P., Wang R.Z., 2010. Numerical heat transfer analysis of the packed bed latent heat storage system based on an effective packed bed model. Energy, vol. 35, pp. 2022-2032.

Xu B., Li P., Chan C., 2015. Application of phase change materials for thermal energy storage in concentrated solar thermal power plants: A review to recent developments. Applied Energy, vol. 160, pp. 286-307.

Yang J., Yang L., Xu C., Du X., 2016. Experimental study on enhancement of thermal energy storage with phase-change material. Applied Energy, vol. 169, pp. 164-176.

Zhang H., Baeyens J., Cáceres G., Degreve J., Lv Y., 2016. Thermal energy storage: Recent developments and practical aspects. Progress in Energy and Combustion Science, vol. 53, pp. 1-40.

Zhao D.L., Li Y., Dai Y.J., Wang R.Z., 2011. Optimal study of a solar air heating system with pebble bed energy storage , Energy Conversion and Management, vol 52, pp. 2392-2400.

Zhao R., Giidwin J.G., Jothimurugesan K., Spivey J.J., Gangwal S.K., 2000. Comparison of attrition test methods: ASTM satandad fluidized bed vs jet cup , Indsutrial and Engineeirng Chemistry Research, vol 39, pp. 1155-1158.

List of Figures

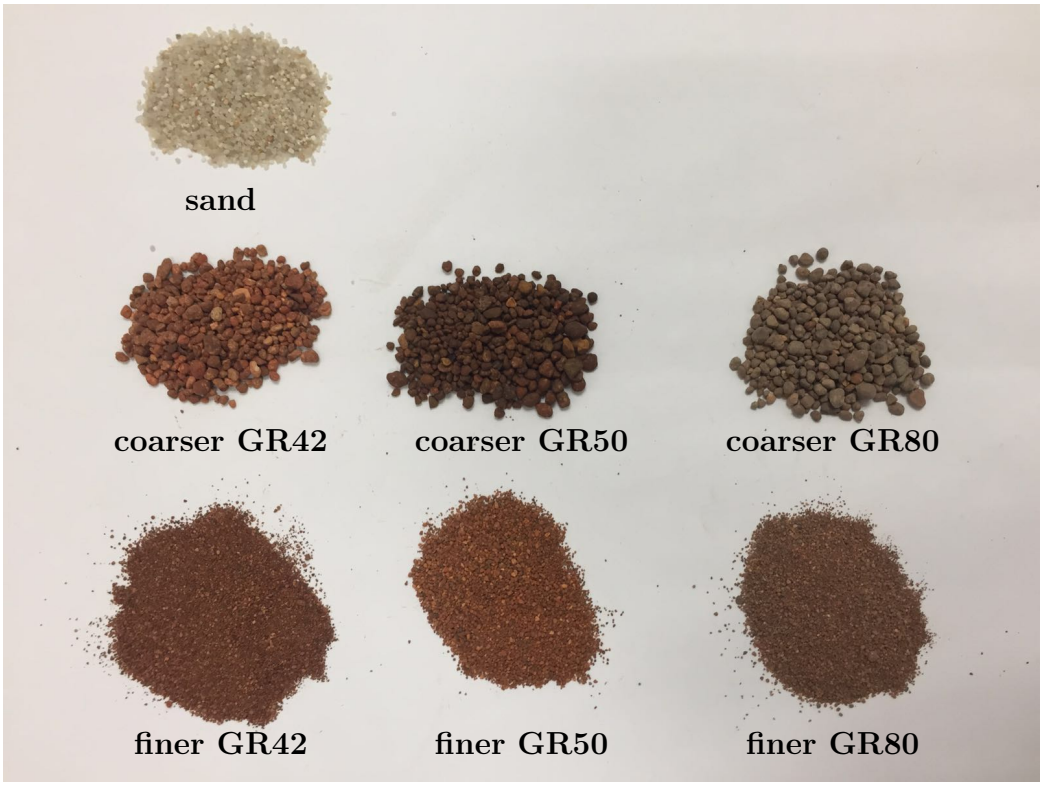

Figure 1: Images of different granular PCMs that are used for sensible heat storage, and silica sand is also shown as a reference .

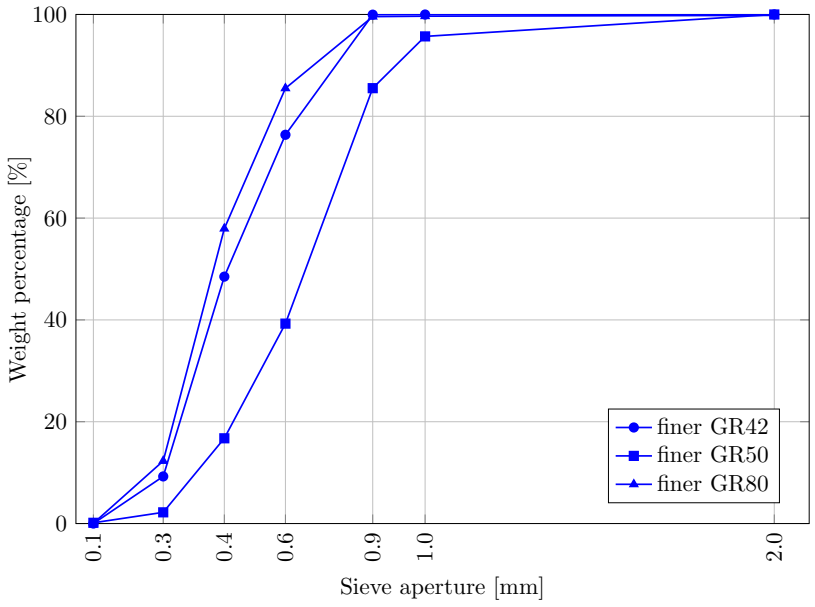

(a)

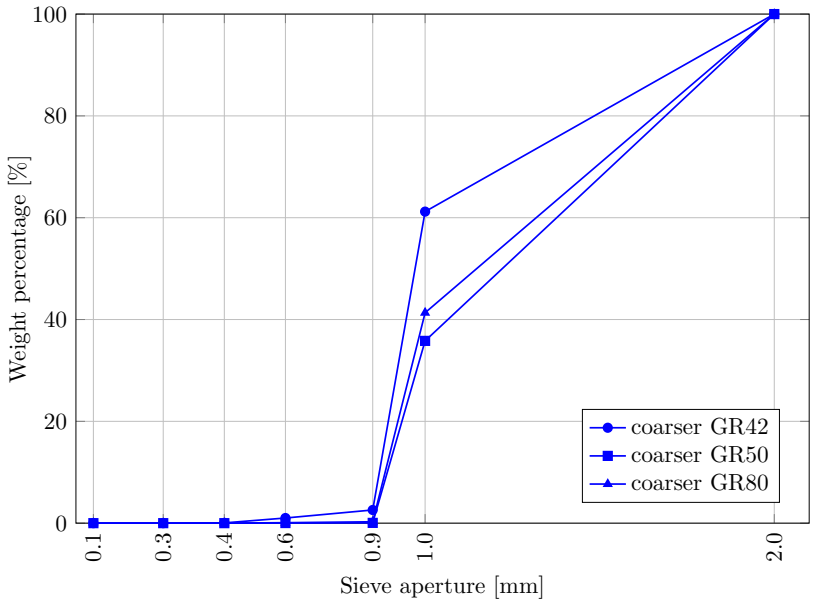

(b)

Figure 2: Particle size distribution of the finer and coarser granular PCMs: GR42, GR50 and GR80.

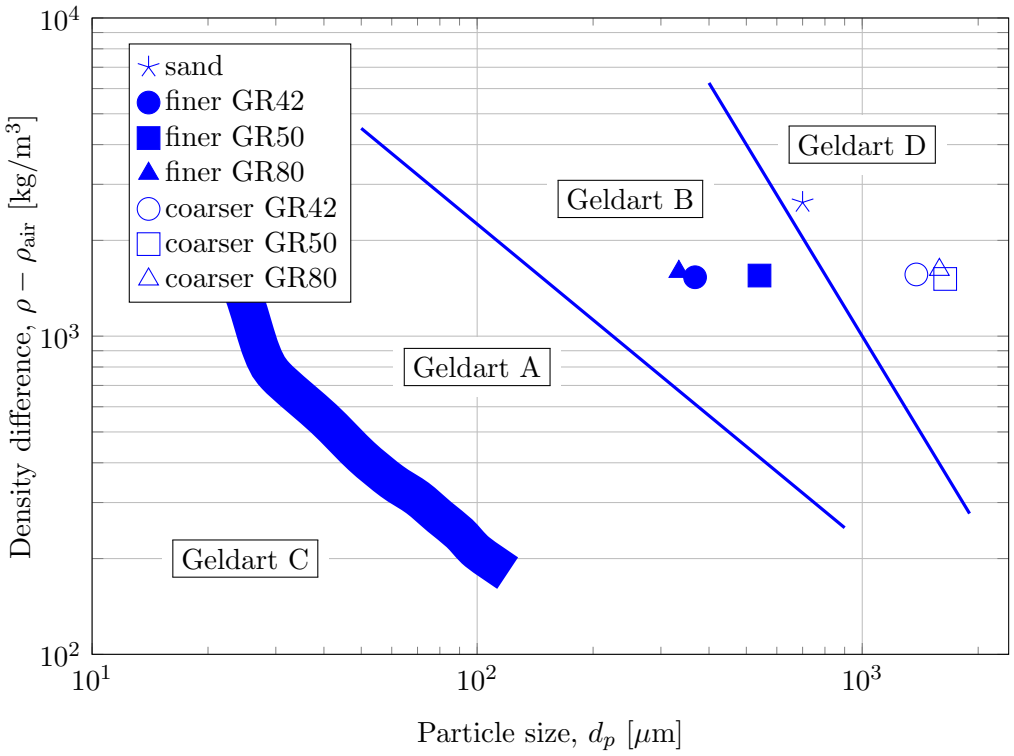

Figure 3: Geldart diagram for particle classification (Geldart, 1973). The symbols indicate the location in the diagram of different granular PCMs in this work and the sand used by Izquierdo-Barrientos et al. (2013).

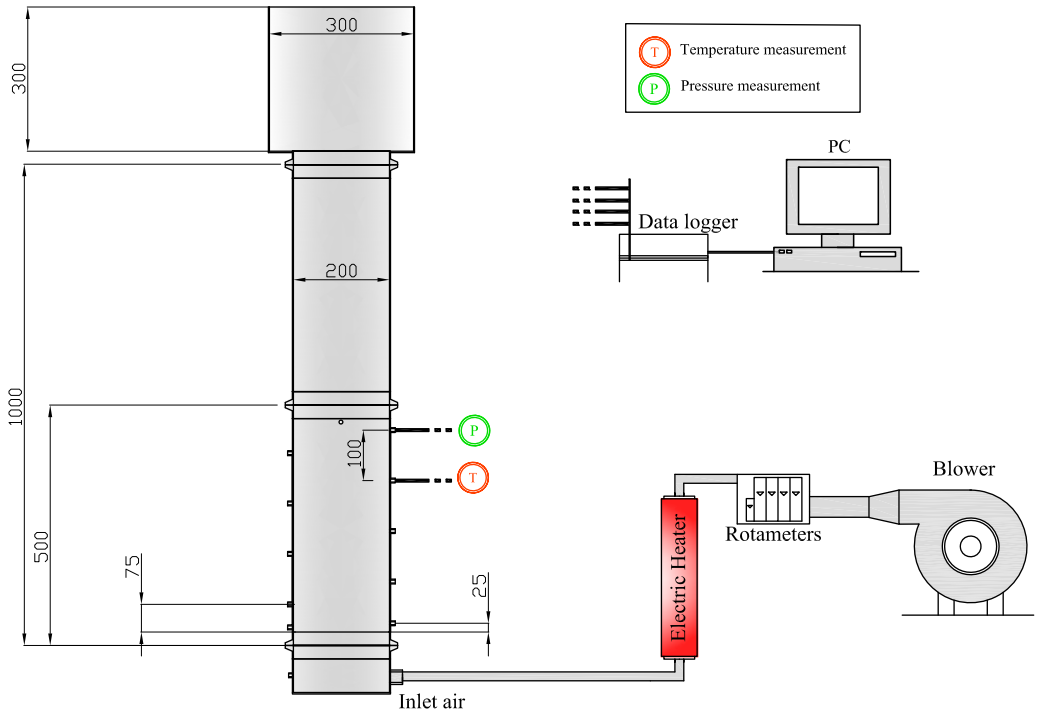

Figure 4: Schematic representation of the 3D-cylindrical fluidized bed. Dimensions in mm.

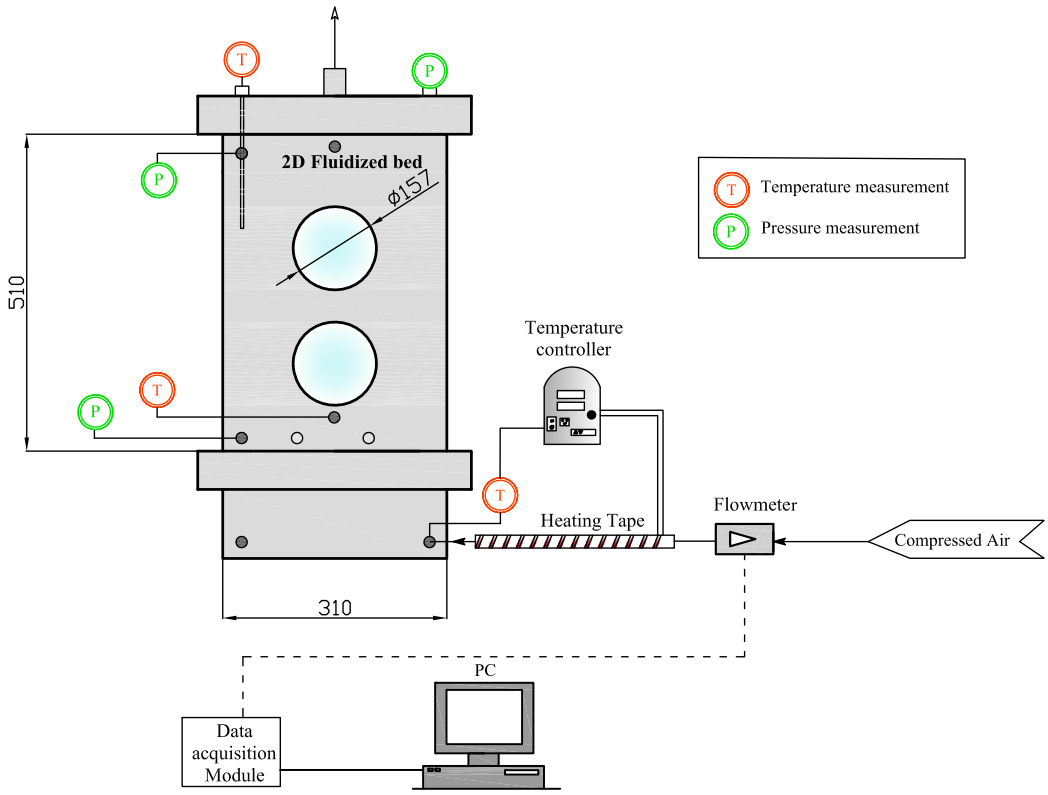

Figure 5: Schematic representation of the planar-2D fluidized bed. Dimensions in mm.

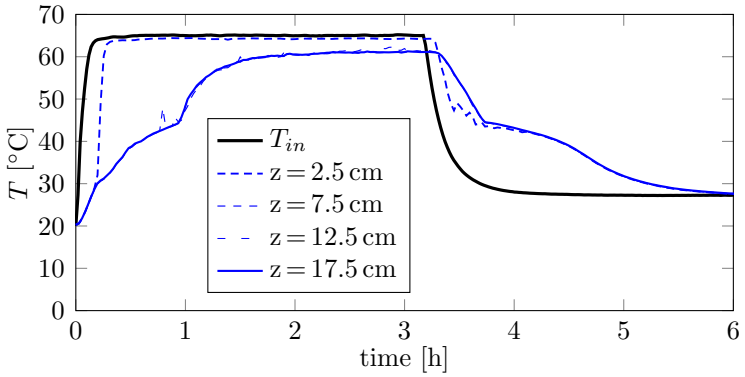

(a) $\dot{V} = 375\,\mathrm{l/min}$, $U/U_{mf} = 1.5$

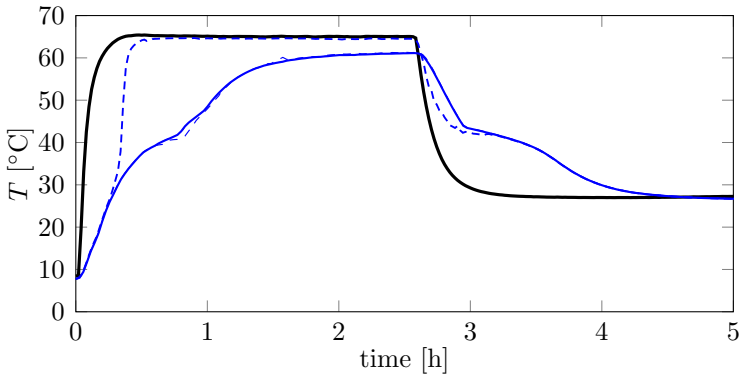

(b) $\dot{V} = 500\,\mathrm{l/min}$, $U/U_{mf} = 2.0$

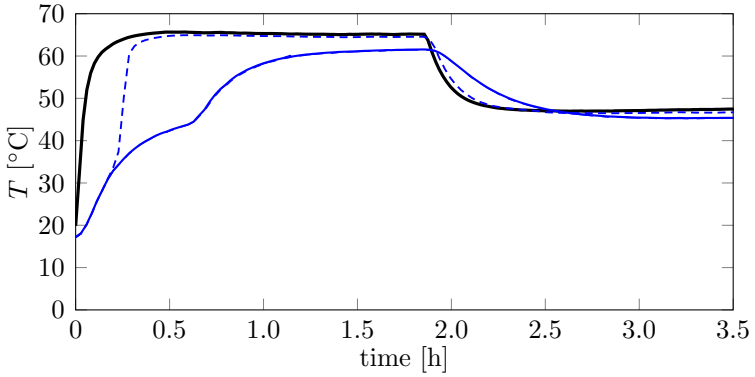

(c) $\dot{V} = 625\,\mathrm{l/min}$, $U/U_{mf} = 2.5$

Figure 6: Temperature variations in the cylindrical-3D bed with the finer GR50. The legend of Figures (b) and (c) is identical to that of Figure (a).

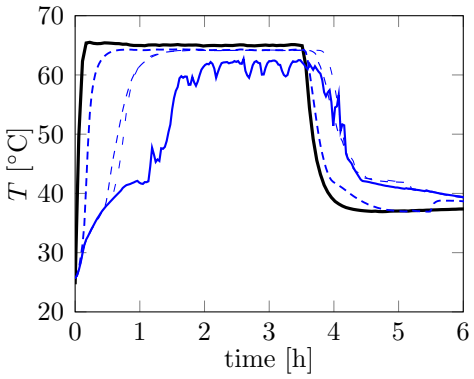

(a) GR42, $\dot{V} = 375\,\mathrm{l/min}$, $U/U_{mf} = 2.1$

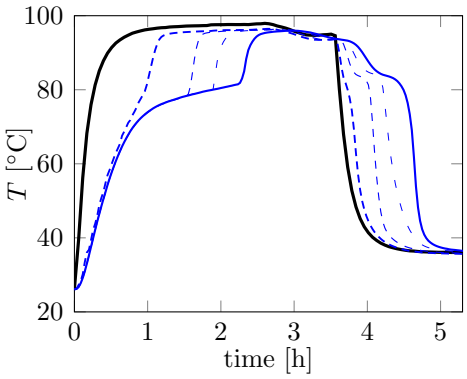

(b) GR80, $\dot{V} = 375\,\mathrm{l/min}$, $U/U_{mf} = 2.6$

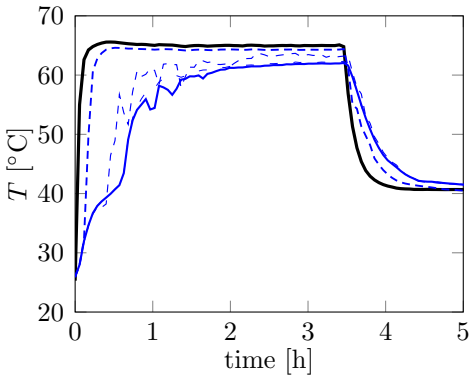

(c) GR42, $\dot{V} = 500\,\mathrm{l/min}$, $U/U_{mf} = 2.8$

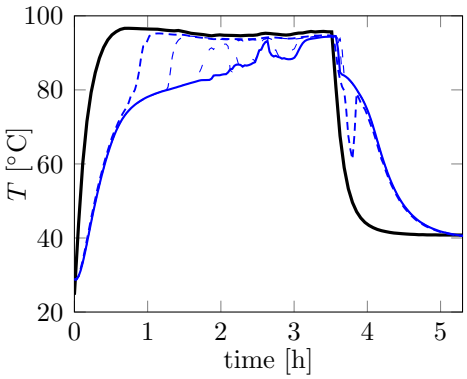

(d) GR80, $\dot{V} = 500\,\mathrm{l/min}$, $U/U_{mf} = 3.5$

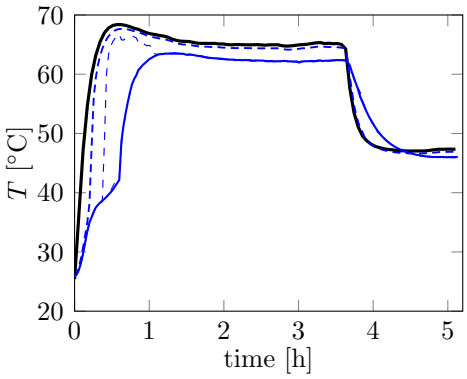

(e) GR42, $\dot{V} = 625\,\mathrm{l/min}$, $U/U_{mf} = 3.5$

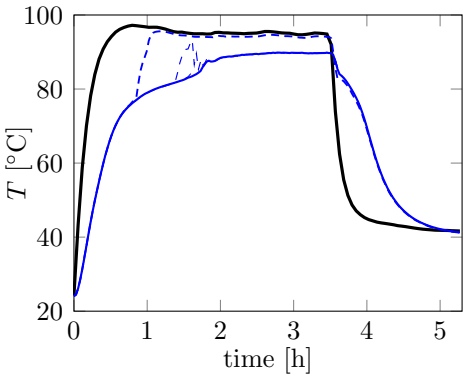

(f) GR80, $\dot{V} = 625\,\mathrm{l/min}$, $U/U_{mf} = 4.4$

Figure 7: Temperature variations in the cylindrical-3D bed with the finer GR42 and GR80. The legend of all figures is identical to that of Figure 6(a).

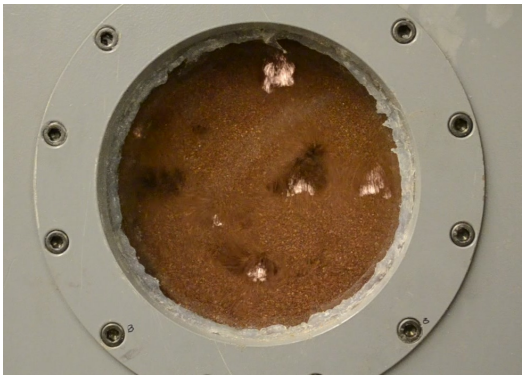

(a) good fluidization ($T < T_{pcm}$ and $U \gtrsim U_{mf}$)

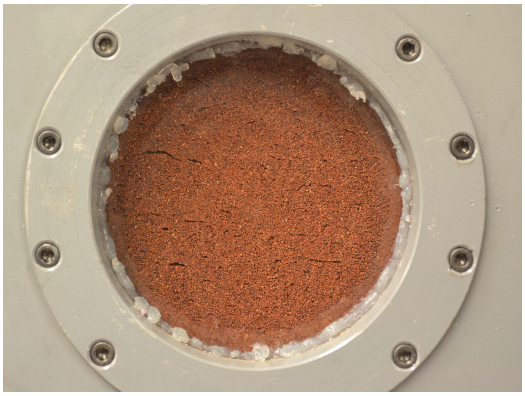

(b) agglomeration ($T > T_{pcm}$ and $U \gtrsim U_{mf}$)

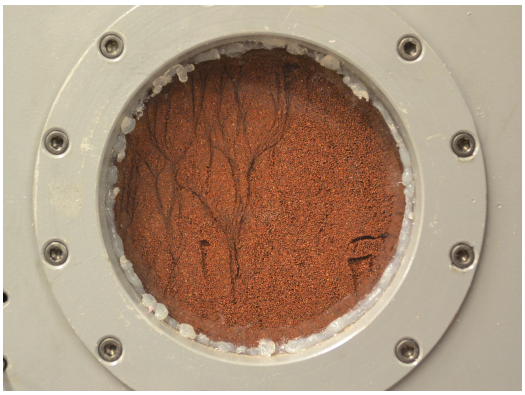

(c) channeling ($T > T_{pcm}$ and $U \gg U_{mf}$)

Figure 8: Visual observation of the fluidization process of the finer GR42.

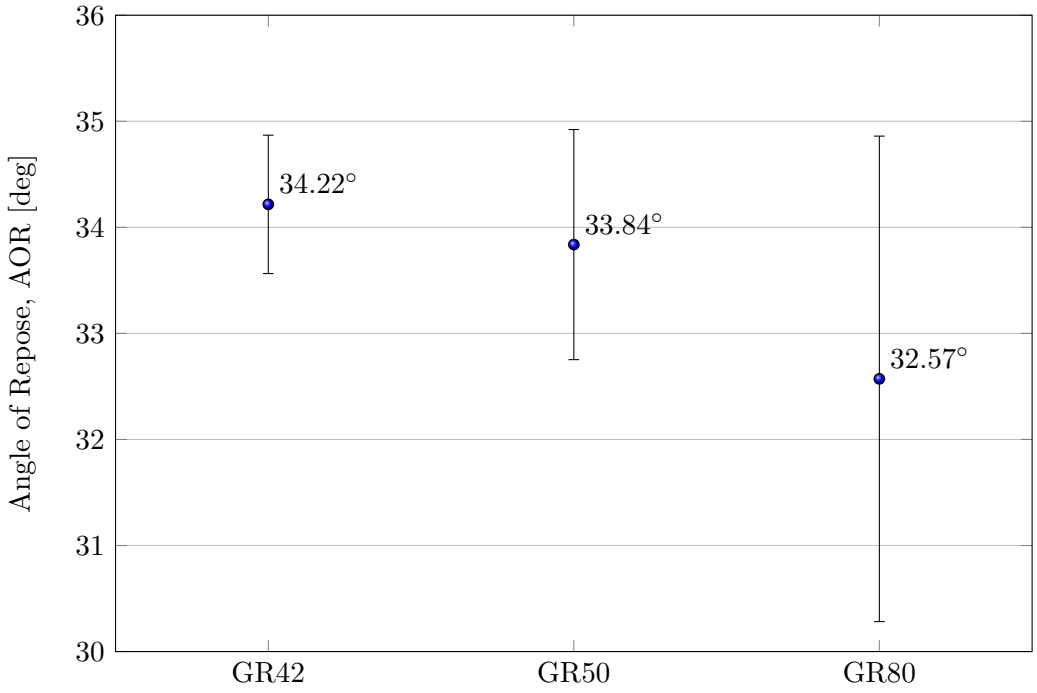

Figure 9: Angle of repose of the three finer granular PCMs at room temperature.

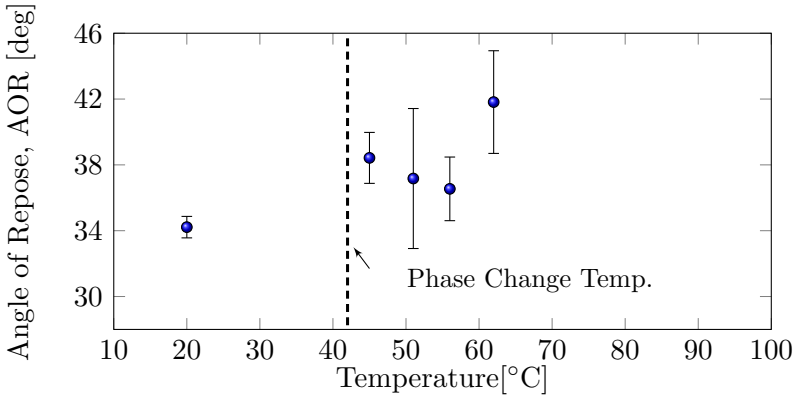

(a) GR42

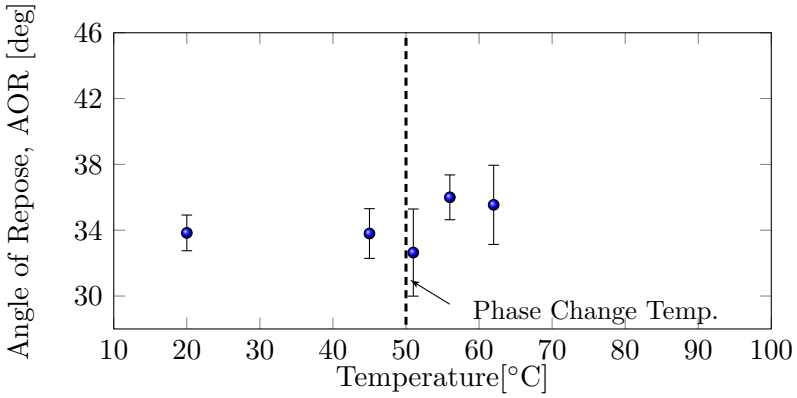

(b) GR50

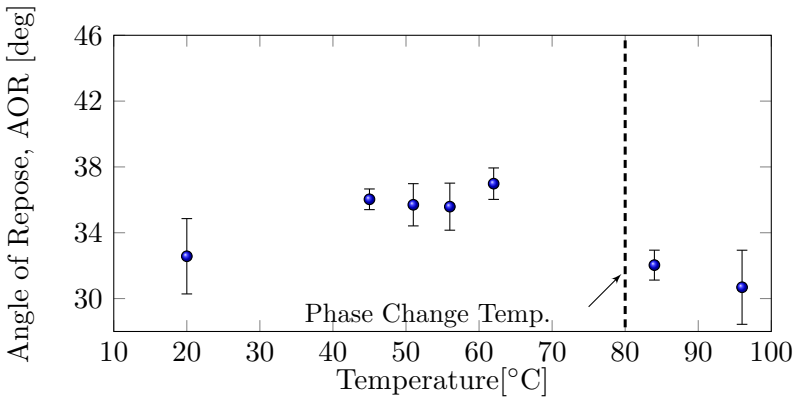

(c) GR80

Figure 10: Variation of the angle of repose with temperature for the three materials.

(a) Blocks

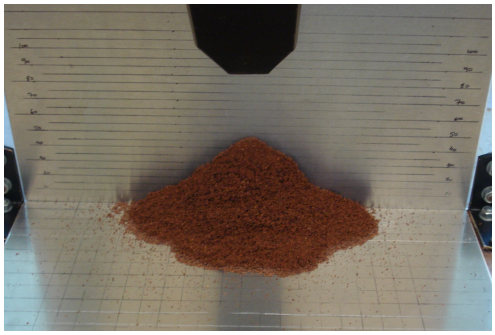

(b) Agglomeration

(c) Electrostatics

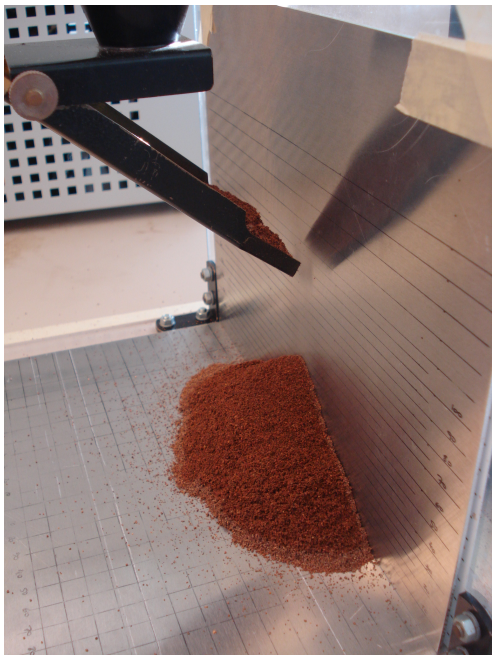

(d) Material stuck

Figure 11: Different problems observed during the angle-of-repose measurement.

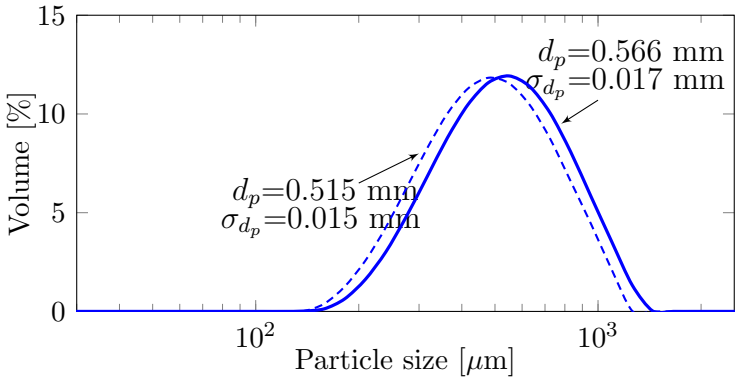

(a) GR42

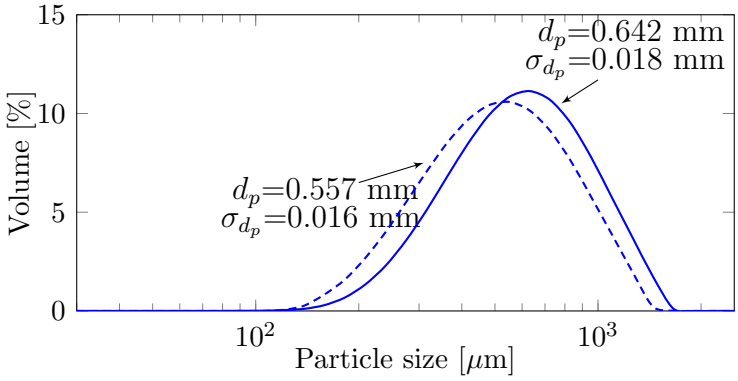

(b) GR50

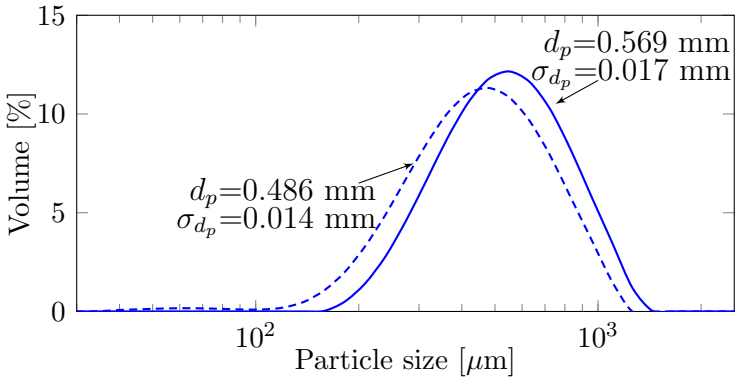

(c) GR80

Figure 12: Particle size distributions of (a) GR42, (b) GR50 and (c) GR80 before (continuous line) and after (dashed line) the attrition tests.

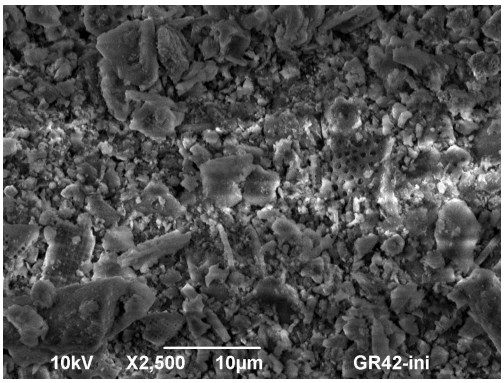

(a) Initial GR42

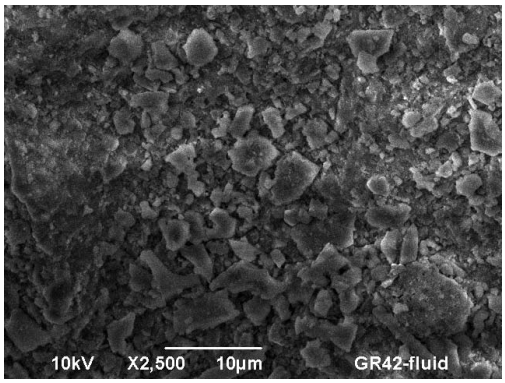

(b) Fluidized GR42

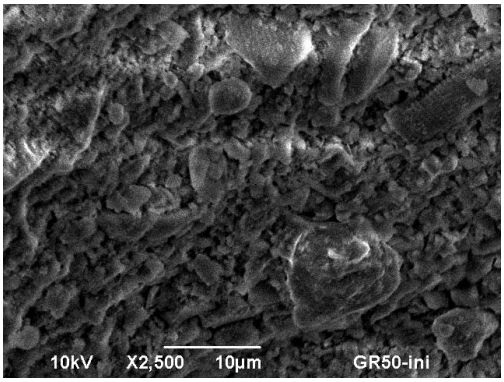

(c) Initial GR50

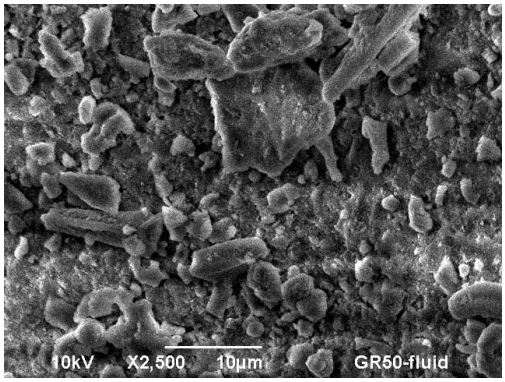

(d) Fluidized GR50

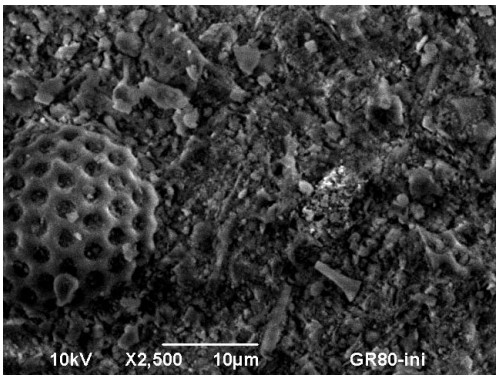

(e) Initial GR80

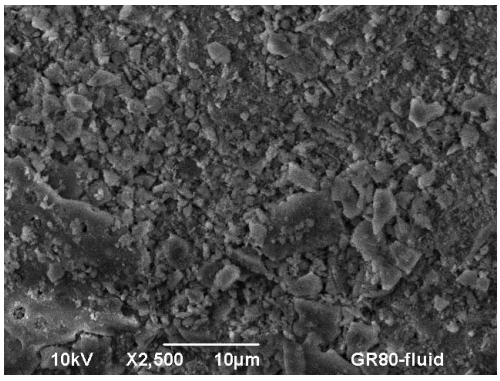

(f) Fluidized GR80

Figure 13: SEM pictures before and after fluidization for the materials (a,b) GR42, (c,d) GR50 and (e,f) GR80.

List of Tables

	Sand	
	$\rho = 2632.3 \pm 1.2$	
	Granular PCM	
	Finer PCM	**Coarser PCM**
GR42	$\rho = 1531.7 \pm 0.7$	$\rho = 1563.1 \pm 0.4$
GR50	$\rho = 1550.5 \pm 1.0$	$\rho = 1512.8 \pm 1.6$
GR80	$\rho = 1594.7 \pm 1.6$	$\rho = 1618.0 \pm 0.3$

Table 1: Density [kg/m^3] of the different granular PCM tested in this work. The density of the sand used by Izquierdo-Barrientos et al. (2013) is also indicated.

	Sand	
	$d_p = 0.755 \pm 0.069$	
	Granular PCM	
	Finer PCM	**Coarser PCM**
GR42	$d_p = 0.368 \pm 0.066$	$d_p = 1.382 \pm 0.202$
GR50	$d_p = 0.541 \pm 0.082$	$d_p = 1.642 \pm 0.196$
GR80	$d_p = 0.334 \pm 0.069$	$d_p = 1.586 \pm 0.202$

Table 2: Mean particle size [mm] of different granular PCMs in this work. The mean particle size of the sand used by Izquierdo-Barrientos et al. (2013) is also indicated

	Sand	
	$U_{mf} = 0.33$	
	Granular PCM	
	Finer PCM	**Coarser PCM**
GR42	$U_{mf} = 0.13$	$U_{mf} = 0.55$
GR50	$U_{mf} = 0.09$	$U_{mf} = 0.65$
GR80	$U_{mf} = 0.07$	$U_{mf} = 0.66$

Table 3: Minimum fluidization velocity [m/s] of different tested granular PCMs in this work. The minimum fluidization velocity of the sand used by Izquierdo-Barrientos et al. (2013) is also indicated. The minimum fluidization velocity for the sand and three finer granular PCMs was experimentally measured, whereas that for the three coarser granular PCMs was calculated according to Wen and Yu (1966).

	ΔH_{fus} [kJ/kg]	ΔH_{sol} [kJ/kg]	$T_{\text{peak}_{\text{fus}}}$ [°C]	$T_{\text{peak}_{\text{sol}}}$ [°C]
0 cycles	44	44	47.9	46.5
3 cycles	44	44	45.4	44.1
6 cycles	46	46	45.4	44.0
9 cycles	43	43	45.4	44.0
12 cycles	43	44	45.3	44.2
15 cycles	44	44	45.5	44.1

Table 4: Enthalpy of fusion (ΔH_{fus}) and solidification (ΔH_{sol}) and peak temperature during the fusion ($T_{\text{peak}_{\text{fus}}}$) and solidification ($T_{\text{peak}_{\text{sol}}}$) for different samples of GR50.